Hindawi
Advances in Materials Science and Engineering
Volume 2022, Article ID 8926780, 9 pages
https://doi.org/10.1155/2022/8926780

Research Article

Salt Spray Corrosion of 2060-T8 Al–Li Alloy in an Aggressive Environment

Zhengquan Zhang, Yuling Wang, and Li Liangfeng

School of Materials Science and Engineering, Southwest University of Science and Technology, 59 Qinglong Road, Mianyang, Sichuan 621010, China

Correspondence should be addressed to Zhengquan Zhang; zzqxazhang@163.com

Received 9 February 2022; Revised 4 May 2022; Accepted 1 June 2022; Published 28 June 2022

Academic Editor: Daniela Pilone

The phase and microstructure of corrosion product formed on 2060-T8 Al–Li alloy have been investigated effectively by SEM and XRD after salt spray corrosion. It was found that the corrosion product growth rate can be divided into three stages: the main phases of corrosion product were Al_2O_3, $Al(OH)_3$, and AlOOH phases; as the increasing of salt spray time, the phase angle of $A1_2O_3$ shifts slightly to the left at 31.8°; and the phase angle of $A1_2O_3$ first shifts to the left, then to the right at 38.6°. The formation and evolution model of salt spray droplet was built, and the formation mechanism of corrosion product was also analyzed. This alloy shows a sensitive corrosion performance to the salt spray environment.

1. Introduction

Al–Li alloy is one of the age-hardenable aluminum alloys and is used to reduce the weight, improve the fuel efficiency of aircraft, and increase the payload in the aerospace industry [1–3]. Compared with traditional aluminum alloys, the Al–Li alloy has a great deal of excellent performance, such as lower density, higher elastic modulus, higher specific strength, and more favorable damage tolerance properties [4–7]. 2060 Al–Li alloy, launched in 2011, is considered as a potential candidate for the use at wing/fuselage forgings, lower wing, and fuselage/pressure cabin [1–7].

Al–Li alloys are susceptible to corrosion after prolonged exposure to high-salt or humidity environment, which influences the use for structural applications. The salt fog phenomenon is commonly found in snowy or ocean environment, which usually induces galvanic corrosion and speeds up electrolytic and galvanic corrosion due to the presence of chloride ion [8–16]. To be accepted for production, components must pass a defined number of neutral salt spray corrosion hours [15]. Salt spray corrosion is able to give fast results and reproduce most of the atmospheric corrosion processes; therefore, it is used extensively in many industries, including the aerospace industry [10, 15]. The evaluation criterion is commonly based on the time taken for corrosion product to appear on the sample's surface [12, 15].

The corrosive characterization of AL-Li alloys depends upon the electrochemical property of matrix, feature of intermetallic, their size of phase and distribution composition of homogeneity element [17–26]. Al–Li alloys contain a wide variety of complex secondary precipitates, including Guinier–Preston(GP) zones, $\theta', \theta, \delta', T1, T2, TB, \Omega$, and S [27–37]. As an age-hardenable aluminum alloy, Al–Li alloy is not resistance to localized corrosion due to its deliberately developed heterogeneous microstructure in corrosive environment, which contains chloride ion [4]. Ahmad reported the exfoliation corrosion of alloy 2060 in an aggressive environment and found there were continuous pits along the grain boundaries and intergranular corrosion. White gelatinous corrosion products formed under the grains [4]. Ma et al. investigated the effect of thermo mechanical treatments on local corrosion susceptibility of 2099 Al–Li alloy and found severe localized corrosion was associated with not only localized plastic deformation occurring during cold working but also heterogeneous precipitation of T1 phase. These alloys displayed

crystallographic corrosion morphology, selective attack of grain boundaries, and grain interiors [34, 35]. Macdonald et al. studied the pitting corrosion of 2098 Al–Li alloy, they thought the Al interstitial comprise the majority of the point defects in the barrier layer of this alloy, the formation of a passive layer had lower capacitance, which is associated with the point defect structure of the barrier layer [38]. Queiroz reported the EIS behavior of anodized and primer coated 2198 AL-Li alloy, they found the uncoated surface of this alloy showed higher pitting susceptibility, larger amounts of corrosion products formed on the anodized and primer coated surface of this alloy, and the diffusion was associated with large amounts of porous corrosion products on the exposed surface of this alloy to the corrosive environment [14]. Moreto et al. thought the localized feature of 2198 Al–Li alloy was essentially related to the existence of intermetallic, which was cathodic or anodic in relation to the aluminum matrix, and this alloy presented a higher long-time resistance to pitting corrosion due to the lower limiting cathodic current [21]. Jiang et al. found the intergranular corrosion of 2197Al–Li alloy is caused by the alternate anodic dissolution of T1 and PFZ, and the increase of the size of T1 at grain boundaries and the width of PFZ along grain boundaries lead to an increase in the susceptibility to intergranular corrosion and exfoliation corrosion [22, 23]. Li et al. found at the beginning, the precipitates of T1 and T2 are anodic to the alloy base and corrosion occurs on their surface; the corroded T1 and T2 precipitates become cathodic to the alloy base at a later stage, leading to the anodic dissolution and corrosion of the alloy base at its adjacent periphery [25–27]; they also discovered the electrode conversion of T2 from anode to cathode is more superficial than that of T1, and the corrosion mainly occurs in T2; they speculated the precipitate of θ is cathodic to the alloy base, resulting in the anodic dissolution and corrosion of the alloy base at its adjacent periphery [23, 25], and the precipitate of η containing active element Mg is anodic to the alloy base, anodic dissolution and corrosion occur on its surface [22, 23]; and they deduced the anodic dissolution of S cause its pitting corrosion [23, 25, 29]. Lv found the corrosion resistance of the 2099 Al–Li alloy was improved by grain refinement and refined precipitation phases due to decreasing of electron work function and the forming of thicker passive film [30]. Navaser inferred in the heat affected zone the corrosion attack was pitting corrosion no intergranular corrosion was detected [39]. Ma considered the copper-rich nanoparticles support local cathodic reactions, which support the anodic dissolution of the adjacent aluminum matrix [33, 34].

The variety of corrosion of Al–Li alloys has been publicly reported in the past few decades, however, salt spray corrosion of these alloys has not been extensively studied. In this study, we investigated salt spray corrosion behavior of 2060 Al–Li alloy in an aggressive environment, analyzed phases, and microstructures of corrosion products after salt spray corrosion.

2. Materials and Experimental Procedures

The chemical composition of the 2060-T8 Al–Li alloy is listed in Table 1. The metallographic image of the 2060-T8 alloy after Keller reagent treating is shown in Figure 1, which shows that the alloy is mainly composed of fine equiaxed grain and large elongated grain. Specimens were cut to $10 \times 10 \times 2$ mm3 for salt spray corrosion. The backsides and rims of these specimens were mounted in an epoxy resin, leaving an exposed area of about 1.0 cm^2. Then, these specimens were ground using SiC sandpaper from 600 to 2000 grit and polished using 0.5 μm Al_2O_3 paste, cleaned ultrasonically in ethanol, and finally dried with compressed nitrogen before use. The processes for continuing salt spray corrosion were performed in salt spray chamber with salt fog deposition rate of 1.5 mL/cm2·h in accordance to the given ASTM-B117 standard in an electrolyte solution at room temperature. The electrolyte solution with pH about 4.0 was prepared by mixing 0.3 M borate (buffer material), 0.5 M sodium chloride, and 1L deionized water. After salt spray corrosion, the specimens were saved in a glove chamber.

Table 1: Nominal composition of 2060-T8 Al–Li alloy, wt%.

Element	Cu	Li	Mg	Mn	Zn	Ag	Zr	Al
%	3.95	0.75	0.85	0.3	0.4	0.25	0.1	Balance

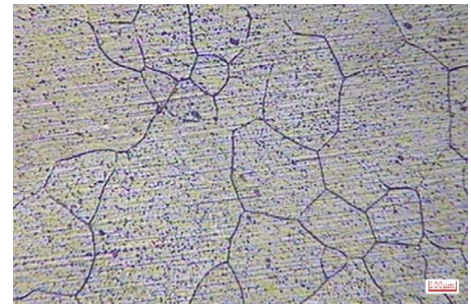

Figure 1: Metallographic image of 2060-T8 alloy after Keller reagent treating.

Before or after salt spray corrosion, the mass of the specimens was weighted by XP 408 weighing balance. The compositions and microstructures of corrosion products formed on 2060-T8 Al–Li alloy after salt spray corrosion were characterized using Carl-Zeiss field emission scanning electron microscope (FE-SEM) at an accelerating voltage of 20 kV equipped with Oxford light elements energy dispersive spectrometry (EDS) detector. The phases of corrosion product were analyzed using PAN analytical model X-ray diffractometer (XRD) with Cu K-radiation between 3° and 90°. Water contact angle tests were performed on a contact angle analyzer (JC2000 C).

3. Results and Discussion

3.1. Formation and Evolution Model of Salt Spray Droplet. Corrosive property is dependent on the presence of chloride ions, which causes pit nucleation; the presence of humidity, which cause galvanic corrosion; and the drying phase, which trap chloride ions beneath the corrosion by-products [13, 40]. The sizes and areas of slat spray droplets can influence the corrosion characterization of 2060-T8 Al–Li alloy. A formation and evolution model of salt spray droplets was established. As shown in Figure 2, at the beginning stage, the

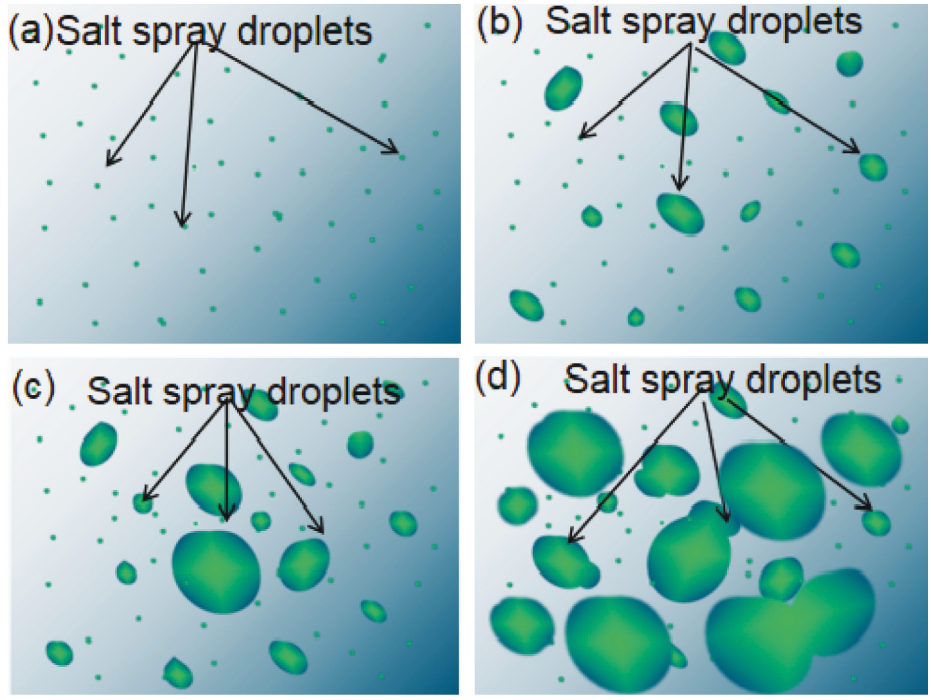

Figure 2: The formation and evolution model of salt spray droplets: (a) salt spray droplets adsorbed and spread on the surface; (b) the smaller salt spray droplets get together to form larger droplets; (c) part of the smaller or larger salt spray droplets deeply get together; (d) most part of the surface was covered with the larger salt spray droplets.

salt spray droplets adsorbed and spread on the surface of this alloy, and the sizes and areas of salt spray droplets were very small and discrete (Figure 2(a))). As salt spray time increases, the sizes and areas of the salt spray droplets increase, because part of the smaller salt spray droplets get together to form larger salt spray droplets (Figure 2(b))). After that, the sizes and areas of the salt spray droplets change much larger, because part of the smaller or larger salt spray droplets deeply get together (Figure 2(c))). Finally, the length, width, and thickness of a single salt spray droplet become larger, so that most parts of the surface were covered with the larger salt spray droplets (Figure 2(d)). The smaller the size, the smaller the coverage area, the lower the chloride ion content, and the fewer corrosion products; the larger the size, the larger the coverage area, the higher the chloride ion content, and the more corrosion products. Water contact angle at different salt spray time is shown in Figure 3. At a short time, the surface is very smooth and a little corrosion product can form, the contact angle is larger. For a long time, the surface is rough, and many corrosion product can form, the contact angle is smaller, which accelerates the attachment of salt spray droplets. As shown in Figure 4, we obtained superficial morphology of Al–Li alloy at different salt spray time, which is accordance to the model of salt spray droplets.

3.2. Mass vs. Time Behavior of Corrosion Product. Mass of corrosion product formed on 2060-T8 Al–Li alloy has been determined by XP 408 weighing balance. As shown in Figure 5, the formation of corrosion product can be divided into three stages during salt spray corrosion. In the first stage

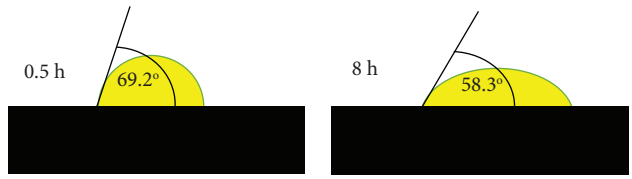

Figure 3: The water contact angle at 0.5 h and 8h.

(from 0.5 to 8 h), the mass of corrosion product increases with a highest slope; in the second stage (from 8 to 32 h), it increases slowly with a lowest slope; in the third stage (from 32 to 72 h), it increases faster than the second stage but slower than the first stage with a medium slope. As we all known, the 2060-T8 Al–Li alloy was covered with a thin layer of contact alumina passive film with Al and O atoms as the main compositions. After the compact alumina film is destroyed, active metal atoms of Al–Li alloys (i.e., Li, Mg) are directly contact with electrolyte solution containing aggressive ions (i.e., Cl-, Br-), which leads to active metal atoms dissolved and corrosion product formed on the alloys [41–43].

3.3. XRD Spectra of Corrosion Products. This passive behavior of Al–Li alloys is attributed to a duplex film, with an inner compact part composed of $Al_2O_3.xH_2O$ and an outer porous part composed of and $Al_2O_3.xH_2O$ [40, 44–49]. XRD spectra was conducted to identify the phase of corrosion product after salt spray corrosion at different time. The XRD patterns of 2060 Al–Li alloy at different time are shown in

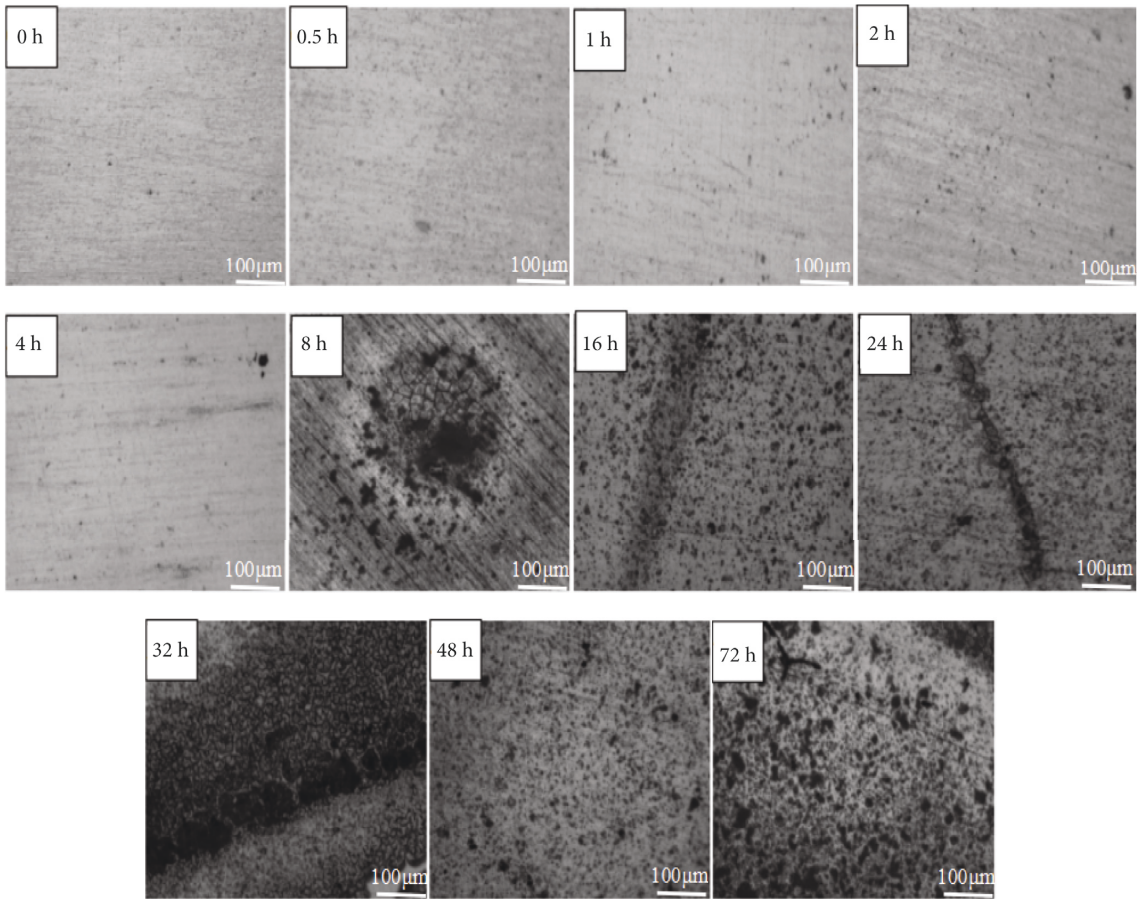

Figure 4: Superficial morphology of Al–Li alloy at different salt spray time.

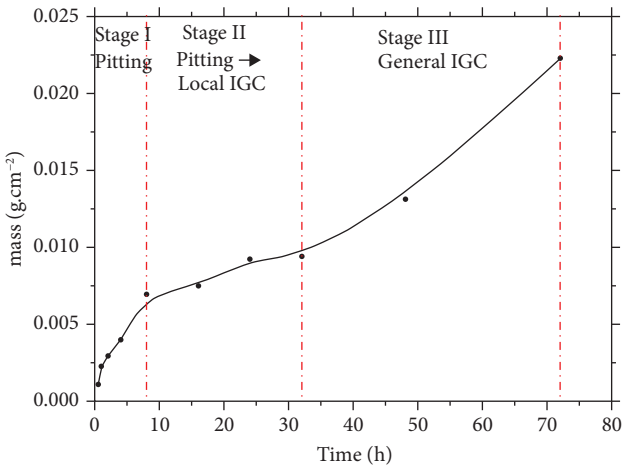

Figure 5: Mass vs. time of corrosion product formed on 2060 Al–Li alloy after salt spray corrosion.

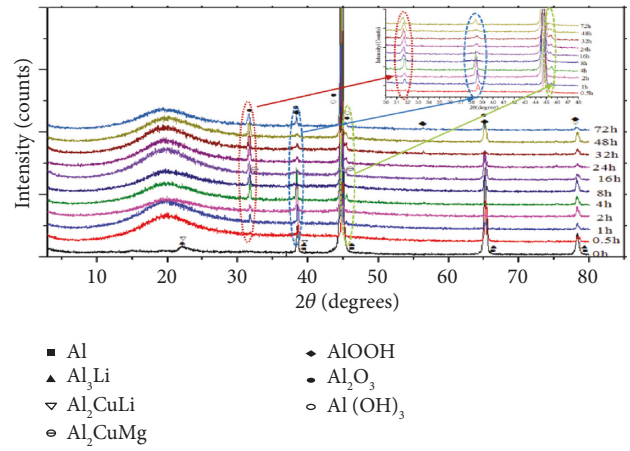

Figure 6: XRD patterns of 2060 Al–Li alloy at different time.

Figure 6. 2060-T8 Al–Li alloy contains a lot of precipitate phases (e.g., δ (Al_3Li), θ(Al_2Cu), T1(Al_2CuLi) and S (Al_2CuMg) phase), which is consistent with reported literature [1–9]. After salt spray corrosion, the diffraction peak of T1 and δ phase disappeared, which means that the first dissolution occurs at T1 or δ phase, as reported in the public literature [19–26]. There are no obvious diffraction peaks from 3 to 25°, which means the presence of amorphous microstructure formed on the surface of this alloy. We discovered that corrosion products mainly contained monoclinic Al_2O_3, aluminum hydroxide cubic $Al(OH)_3$, and hexagonal AlOOH phases. Davo thought the pH increase permits the precipitation of a porous and open $Al(OH)_3$ compounds, which is corresponding to the voluminous nonprotective aluminum oxides/hydroxides [18].

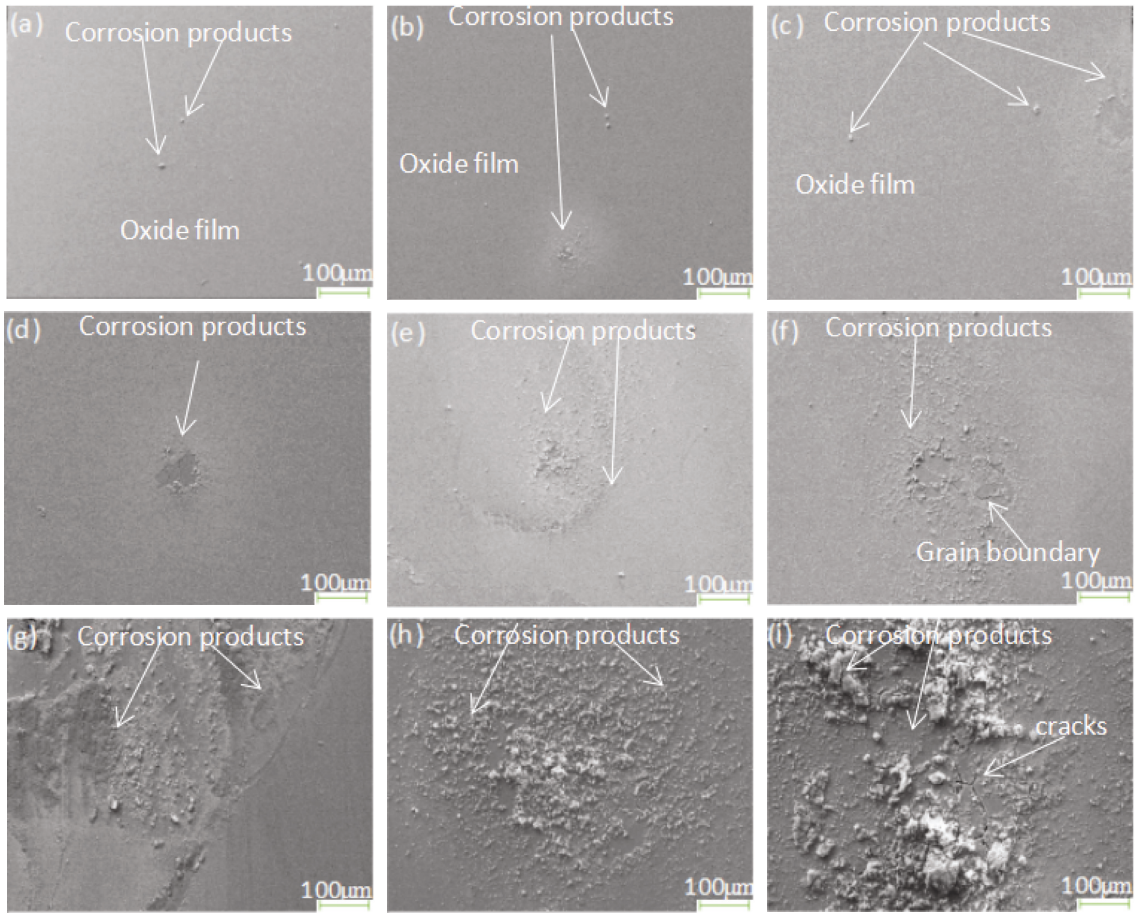

Figure 7: SEM images of corrosion product of 2060 Al–Li alloy after salt spray corrosion at different times: (a) 1, (b) 2, (c) 4, (d) 8, (e) 16, (f) 24, (g) 32, (h) 48, and (i) 72h.

Bockris also discovered that it is of a porous outer layer, which consists predominantly of $Al(OH)_3$ and (Al_2O_3), and an inner layer, which is a mixed crystal of (Al_2O_3) and AlOOH [48]. As the increasing of salt spray time, the phase angle of $A1_2O_3$ shifts slightly to the left at 31.8°. There is a tensile stress in the $A1_2O_3$ layer. As the salt spray time increases, the compact $A1_2O_3$ passivity film becomes thinner, the morphologies changed from compact to porous, resulting in an increase in tensile stress. After 0.5 hour corrosion, no diffraction peak of $A1_2O_3$ was found, we think that there is a crystal phase transition. The phase angle of $A1_2O_3$ or AlOOH first shifts to the left, then to the right at 38.6°; at the same time, the peak intensity first increases and then decreases. We thought at the beginning that the tensile played a leading role. When the time exceeds 4 hours, compressive stress plays a major role. When the salt spray time was less than 4 hours, the AlOOH phase appeared and grew up with time increasing, and then changed into $A1_2O_3$ or $Al(OH)_3$ phase. Therefore, when the corrosion time exceeded 4 hours, diffraction peaks of $Al(OH)_3$ were discovered and Al(OH)3 was formed on the surface of 2060-T8 Al–Li alloy, which is in accordance with the reported [18, 33, 40, 45–49].

3.4. Morphology of Corrosion Products. Individual specimens were examined to determine the surface morphology of corrosion product formed on the 2060-T8 alloy at different salt spray corrosion time. As shown in Figure 7, there was difference in the areas and distributions of corrosion products. After a shorter time, there were almost a few corrosion products formed on this alloy. After salt spray corrosion time over 24h, severe corrosion occurs, and parts of corrosion products peeled off from the surface of specimen. Spalling corrosion products accumulated on the surface of this alloy, and cracks in the form of mud-cracking were found on the surface of alloys. The oxidation film exposed to salt spray as a sacrificial anode to protect basic metal. The gelatinous $Al(OH)_3$, which is pumped out by pits dries up eventually and cracks [25–28]. The corrosion products covered the cracks and pores so that the numbers of the cracks and pores seemed apparently smaller. Cheng et al. thought it may be a result of continuous dissolution of the metal elements on the alloy surface [1, 37]. Meanwhile, chloride anions migrate from surface electrolytes into corrosion product layer to keep electrical neutrality and lead to form second powdery aspect corrosion products on the top of corrosion cracks. Gharbi proposed a highly

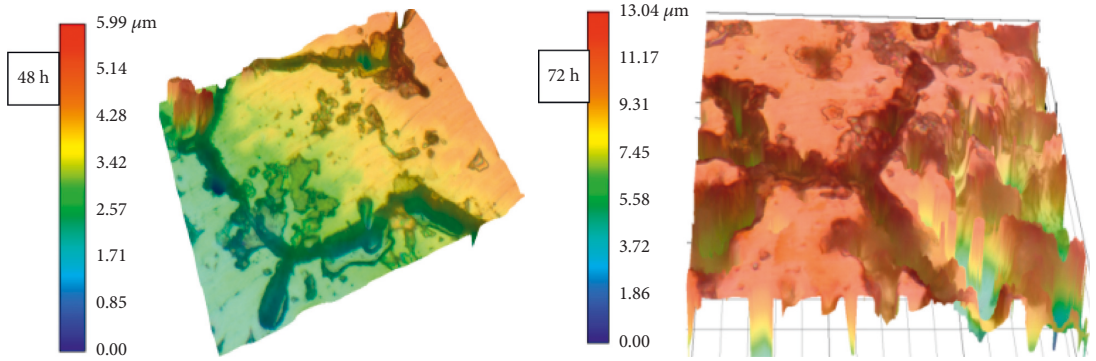

Figure 8: Image of three-dimensional (3D) profiles of sample surfaces.

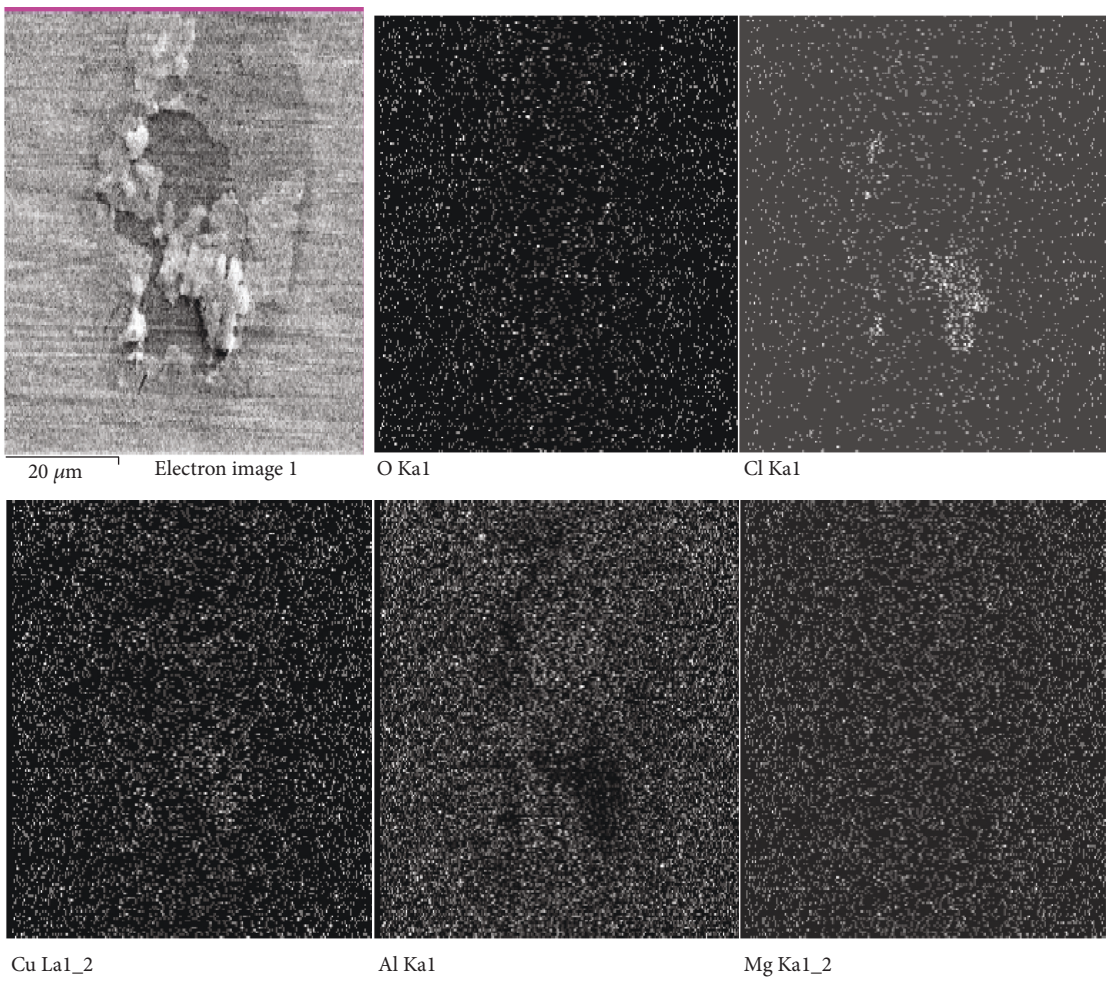

Figure 9: Element distribution map at 1 hour.

heterogeneous surface, with the evidence of surface mud or cracking feature, was induced by the dehydration of the hydroxide film or several precipitate particles on the surface [28]. Ma thought the distribution of surface cracks also depends on grain orientation [33, 34]. Local breakdown of some corrosion products leads to abrupt potential drops, which associated with an initiation of localized corrosion attack along the grain boundaries. Network cracking of corrosion products appears at part of specimen. It is believed that the cracks were introduced after water evaporation [30]. Subsequently, the corrosion products represented as dry mud grooves or cracking feature [18]. Cheng et al. thought it may be a result of continuous dissolution of the metal elements on the alloy surface [1, 37]. Meanwhile, chloride anions migrate from surface electrolytes into corrosion product layer to keep electrical neutrality and lead to form second powdery aspect corrosion products on the top of corrosion cracks. Gharbi proposed a highly heterogeneous

surface, with the evidence of surface mud or cracking feature, was induced by the dehydration of the hydroxide film or several precipitate particles on the surface [28]. Ma et al. thought the distribution of surface cracks also depends on grain orientation [33, 34]. We obtained the three-dimensional (3D) images at 48h and 72h to reveal the surface of the localized corroded areas, as shown in Figure 8, which displayed that the time of salt spray droplet had an effect on depth of corrosion. We found that the time was shorter, the depth of pit cavity was less. As shown in Figure 9, we have performed the surface elemental distribution analysis on the surface of Al–Li alloy, we found that the surface elements were Mg,O, Cu, Cl, and Al, which showed the corrosion product formed on the surface.

4. Formation Mechanism of Corrosion Product

The salt spray droplets dissolving a lot of chloride ions, which can adhere, spread out, and cover the most surface of 2060-T8 Al–Li alloy, as shown in Figure 1. The chloride ions can migrate from the solution to the passivity film, break down the compact passivity film, resulting in active metal atoms directly exposed to chloride ions and the corrosion occurrence on the surface of this alloy. In the initial corrosion process, the pH value is lower, anodic reaction occurs due to the first dissolution of T1 or δ phase. The dissolution mechanism of this alloy in an acid condition is as follows [40–49]:

$$\mathrm{Li}\ (ss) \longrightarrow \mathrm{Li} + (aq) + \mathrm{e}^- \tag{1}$$

$$\mathrm{H_2O} \longrightarrow \mathrm{H^+}\,(aq) + \mathrm{OH^-}\,(aq) \tag{2}$$

where H^+(aq) is the hydrogen ion in the aqueous solution, OH^-(aq) represents the hydroxyl ion in the aqueous solution, and Li(ss) is the active element in the T1, T2, or δ phase.

After the active Li element disappears, amounts of hydrogen ions are consumed and gas bubbles are generated, which makes the value of pH increases [4]. H_2(g) is the gas due to the galvanic chemical reactivity.

$$\mathrm{H} + (aq) + e^- \longrightarrow \mathrm{H_2}\,(g)\uparrow \tag{3}$$

When the aluminum element in this alloy matrix begins to be dissolved, and transfers into solution, it causes the aluminum matrix to be corroded [40–50].

$$\mathrm{AI^+}\,(ss) \longrightarrow \mathrm{AI^{3+}}\,(aq) + 3e^- \tag{4}$$

After the aluminum ions migrate into the solution, aluminum ions react with hydroxyl ion, in a short time, the content of hydroxyl ion in solution is lower, resulting in forming $AlOH_2$+. The reaction is as follows:

$$\mathrm{AI^{3+}} + \mathrm{OH^-} \longrightarrow \mathrm{AIOH^{2+}} \tag{5}$$

The content of hydroxyl ion and the value of pH in solution increase with the time increasing, then AlOOH is formed, as shown in Figure 3, and the reaction is

$$\mathrm{AI^{3+}} + \mathrm{OH^-} \longrightarrow \mathrm{AIOOH} + \mathrm{H^+} \tag{6}$$

At the same time, the reaction is occurring:

$$\mathrm{AIOH^{2+}} + \mathrm{Cl^-} \longrightarrow \mathrm{AlOHCl^+} \tag{7}$$

$$\mathrm{AlOHCl^+} + \mathrm{Cl^-} \longrightarrow \mathrm{AlOHCl_2} \tag{8}$$

When the value of pH exceeds 7, the $Al(OH)_3$ phase can be formed, as shown in Figure 6:

$$\mathrm{AlOHCl^+} + 2\mathrm{OH^-} \longrightarrow \mathrm{Al(OH)_3} + \mathrm{Cl^-} \tag{9}$$

$$\mathrm{AlOHCl_2} + \mathrm{Cl^-} \longrightarrow \mathrm{AlCl_3} + \mathrm{OH^-} \tag{10}$$

$$\mathrm{AlCl_3} + 3\mathrm{H_2O} \longrightarrow \mathrm{Al(OH)_3} + 3\mathrm{HCl} \tag{11}$$

The $Al(OH)_3$ phase may come from the AlOOH phase, and the reaction is

$$\mathrm{AlOOH} + \mathrm{H_2O} \longrightarrow \mathrm{Al(OH)_3} \tag{12}$$

The $Al(OH)_3$ can decompose into Al_2O_3, and the reaction is as follows:

$$2\mathrm{Al(OH)_3} \longrightarrow \mathrm{Al_2O_3} + 3\mathrm{H_2O} \tag{13}$$

5. Conclusions

(1) The corrosion product growth rate can be divided into three stages: in the first stage, it increased exponentially with time during the first 8 h; in the second stage, it increased linearly with a lower slope from 8 to 32 h; and, in the last stage, it changed linearly with a higher slope than the second stage from 32 to 72h.

(2) The main phases of corrosion products were Al_2O_3, $Al(OH)_3$, and AlOOH phases. As the increasing of salt spray time, the phase angle of $A1_2O_3$ shifts slightly to the left at 31.8°, and the phase angle of $A1_2O_3$ first shifts to the left, then to the right at 38.6°.

Data Availability

All data generated or analyzed during this study are included in this published article.

Conflicts of Interest

The authors declare that they have no conflicts of interest.

Acknowledgments

All authors contributed equally to this work. The authors thank Professor Xingquan Zhang, Professor Kaibing Fu, and Professor Jinlong Tang for their help in this work.

References

[1] X. C. Xu, D. X. Liu, Y. Y. Guan, S. M. Cheng, and H. B. Liu, "Effect of the shot peening on the surface integrity and fatigue property of 2060 aluminum lithium alloy," *Mechanical Science*

and Technology for Aerospace Engineering, vol. 35, pp. 1444–1449, 2016.

[2] J. F. Sun, Z. Q. Zheng, Y. Lin, D. Q. He, H. P. Li, and Q. P. Wu, "Microstructures and mechanical properties of 2060 alloy FSW joint," *Chinese Journal of Nonferrous Metals*, vol. 24, pp. 364–370, 2014.

[3] M. C. Yang, Z. G. Sun, R. Ma, Q. Meng, and J. Chen, "Analysis for microstructure and precipitation phase evolution of friction stir welding 2060 butt joint," *Materials Science and Technology*, vol. 22, pp. 119–123, 2014.

[4] A. I. Karayan, K. Jata, M. Velez, and H. Castaneda, "On exfoliation corrosion of alloy 2060 T8E30 in an aggressive acid environment," *Journal of Alloys and Compounds*, vol. 657, pp. 546–558, 2016.

[5] J. Xiao Jin, B. Q. Fu, C. l. Zhang, C. L. Zhang, and W. Liu, "Strain localization and damage development in 2060 alloy during bending," *International Journal of Minerals, Metallurgy and Materials*, vol. 22, no. 12, pp. 1313–1321, 2015.

[6] X. Zhan, C. Gu, H. L. Wu et al., "Experimental and numerical analysis on the strength of 2060Al-Li alloy adhesively bonded T joints," *International Journal of Adhesion and Adhesives*, vol. 65, pp. 79–87, 2016.

[7] X. Y. Zhang, W. X. Yang, and R. S. Xiao, "Microstructure and mechanical properties of laser beam welded Al-Li alloy 2060 with Al-Mg filler wire," *Materials & Design*, vol. 88, pp. 446–450, 2015.

[8] A. G. Gracia, H. Frémont, B. Plano, J. Y. Delétag, and K. W. Zaage, "Effects of salt spray corrosion on lead-free solder alloy," *Microelectronics eliability*, vol. 64, 2016.

[9] I. Daisuke, A. Yoshikazu, M. Yoshikazu, Y. Takashi, and O. Shinji, "Evaluation of degradation of high performance organic coatings under outdoor salt spray corrosion," *ECS Transactions*, vol. 50, pp. 37–42, 2013.

[10] E. D. Kiosidou, A. Karantonis, D. I. Pantelis, E. R. Silva, and J. C. M. Bordado, "Rust morphology characterization of polyurethane and acrylic-based marine antifouling paints after salt spray test on scribed specimens," *Journal of Coatings Technology and Research*, vol. 14, no. 6, pp. 1381–1395, 2017.

[11] H. H. Man, H. C. Man, and L. K. Leung, "Corrosion protection of NdFeB magnets by surface coatings - Part I: salt spray test," *Journal of Magnetism and Magnetic Materials*, vol. 152, no. 1-2, pp. 40–46, 1996.

[12] S. Manivannan, P. Dinesh, S. K. Babu, and S. Sundarrajan, "Investigation and corrosion performance of cast Mg-6Al-1Zn+xCa alloy under salt spray test (ASTM-B117)," *Journal of Magnesium and Alloys*, vol. 3, no. 1, pp. 86–94, 2015.

[13] N. I. M. Nordin, S. M. Said, R. Ramli et al., "Microstructure of Sn-1Ag-0.5Cu solder alloy bearing Fe under salt spray Test," *Microelectronics Reliability*, vol. 54, no. 9-10, pp. 2044–2047, 2014.

[14] F. M. Queiroz, A. F. S. Bugarin, N. P. Hammel, V. R. Capelossi, M. Terada, and I. Costa, "EIS behavior of anodized and primer coated AA2198-T851 compared to AA2024-T3 exposed to salt spray CASS test," *Surface and Interface Analysis*, vol. 48, no. 8, pp. 755–766, 2016.

[15] S. Cecchel, G. Cornacchia, and M. Gelfi, "A study of a non-conventional evaluation of results from salt spray test of aluminum high pressure die casting alloys for automotive components," *Materials and Corrosion*, vol. 70, no. 1, pp. 70–78, 2019.

[16] Y. P. Wu, S. F. Zhu, P. Shi, B. J. Yan, D. Z. Cai, and Y. Zhang, "Corrosion behavior of Al film on uranium in salt spray test," *RSC Advances*, vol. 7, no. 25, pp. 14981–14988, 2017.

[17] A. Chen, L. Zhang, G. Wu, M. Sun, and W. Liu, "Influences of Mn content on the microstructures and mechanical properties of cast Al-3Li-2Cu-0.2Zr alloy," *Journal of Alloys and Compounds*, vol. 715, pp. 421–431, 2017.

[18] B. Davo´ and J. J. de Damborenea, "Use of rare earth salts as electrochemical corrosion inhibitors for an Al-Li-Cu (8090) alloy in 3.56% NaCl," *Electrochimica Acta*, vol. 49, no. 27, pp. 4957–4965, 2004.

[19] H. Y. Li, Y. Tang, Z. D. Zeng, and F. Zheng, "Exfoliation corrosion of T6- and T8-aged AlxCuyLiz alloy," *Transactions of Nonferrous Metals Society of China*, vol. 18, no. 4, pp. 778–783, 2008.

[20] H. L. Qin, H. Zhang, and H. Q. Wu, "The evolution of precipitation and microstructure in friction stir welded 2195-T8Al-Li alloy," *Materials Science and Engineering A*, vol. 626, pp. 322–329, 2015.

[21] J. A. Moreto, C. E. B. Marino, W. W. Bose Filho, L. A. Rocha, and J. C. S. Fernandes, "SVET, SKP and EIS study of the corrosion behaviour of high strength Al and Al–Li alloys used in aircraft fabrication," *Corrosion Science*, vol. 84, pp. 30–41, 2014.

[22] N. Jiang, J. F. Li, Z. Q. Zheng, X. Y. Wei, and Y. F. Li, "Effect of aging on mechanical properties and localized corrosion behaviors of Al-Cu-Li alloy," *Transactions of Nonferrous Metals Society of China*, vol. 15, pp. 23–29, 2005.

[23] J. F. Li, Z. Ziqiao, J. Na, and T. Chengyu, "Localized corrosion mechanism of 2×××-series Al alloy containing S (Al2CuMg) and θ'(Al2Cu) precipitates in 4.0% NaCl solution at pH 6.1," *Materials Chemistry and Physics*, vol. 91, no. 2-3, pp. 325–329, 2005.

[24] J. Zhong, S. Zhong, Z. Q. Zheng, H. F. Zhang, and X. F. Luo, "Fatigue crack initiation and early propagation behavior of 2A97 Al-Li alloy," *Transactions of Nonferrous Metals Society of China*, vol. 24, no. 2, pp. 303–309, 2014.

[25] J. F. Li, Z. Q. Zheng, W. D. Ren, W. J. Chen, X. S. Zhao, and S. C. Li, "Simulation on function mechanism of T1 (Al2CuLi) precipitate in localized corrosion of Al-Cu-Li alloys," *Transactions of Nonferrous Metals Society of China*, vol. 16, no. 6, pp. 1268–1273, 2006.

[26] X. L. Zhang, L. Zhang, G. H. Wu et al., "Microstructural evolution and mechanical properties of cast Al-2Li-2Cu-0.5Mg-0.2Zr alloy during heat treatment," *Materials Characterization*, vol. 132, pp. 312–319, 2017.

[27] J. F. Li, C. X. Li, Z. W. Peng, W. J. Chen, and Z. Q. Zheng, "Corrosion mechanism associated with T1 and T2 precipitates of Al-Cu-Li alloys in NaCl solution," *Journal of Alloys and Compounds*, vol. 460, no. 1-2, pp. 688–693, 2008.

[28] O. Gharbi, N. Birbilis, and K. Ogle, "Li reactivity during the surface pretreatment of Al-Li alloy AA2050-T3," *Electrochimica Acta*, vol. 243, pp. 207–219, 2017.

[29] J. F. Li, Z. Q. Zheng, S. C. Li, W. J. Chen, W. D. Ren, and X. S. Zhao, "Simulation study on function mechanism of some precipitates in localized corrosion of Al alloys," *Corrosion Science*, vol. 49, no. 6, pp. 2436–2449, 2007.

[30] L. Jinlong, L. Tongxiang, W. Chen, and G. Ting, "The passive film characteristics of several plastic deformation 2099 Al-Li alloy," *Journal of Alloys and Compounds*, vol. 662, pp. 143–149, 2016.

[31] Q. Liu, R. H. Zhu, J. F. Li et al., "Microstructural evolution of Mg, Ag and Zn micro-alloyed Al-Cu-Li alloy during homogenization," *Transactions of Nonferrous Metals Society of China*, vol. 26, no. 3, pp. 607–619, 2016.

[32] X. Y. Zhang, T. Huang, W. X. Yang, R. S. Xiao, Z. Liu, and L. Li, "Microstructure and mechanical properties of laser

beam-weldedAA2060 Al-Li alloy," *Journal of Materials Processing Technology*, vol. 237, pp. 301–308, 2016.

[33] Y. Ma, X. Zhou, G. E. Thompson et al., "Anodic film growth on Al-Li-Cu alloy AA2099-T8," *Electrochimica Acta*, vol. 80, pp. 148–159, 2012.

[34] Y. Ma, X. Zhou, G. E. Thompson, and P. Skeldon, "Surface texture formed on AA2099 Al-Li-Cu alloy during alkaline etching," *Corrosion Science*, vol. 66, pp. 292–299, 2013.

[35] Y. L. Ma, X. R. Zhou, X. M. Meng et al., "Influence of thermomechanical treatments on localized corrosion susceptibility and propagation mechanism of AA2099 Al–Li alloy," *Transactions of Nonferrous Metals Society of China*, vol. 26, no. 6, pp. 1472–1481, 2016.

[36] Y. Lin, Z. Q. Zheng, S. C. Li, X. Kong, and Y. Han, "Microstructures and properties of 2099 Al-Li alloy," *Materials Characterization*, vol. 84, pp. 88–99, 2013.

[37] Y. L. Cheng, M. K. Mao, J. H. Cao, and Z. M. Peng, "Plasma electrolytic oxidation of an Al-Cu-Li alloy in alkaline aluminate electrolytes: a competition between growth and dissolution for the initial ultra-thin films," *Electrochimica Acta*, vol. 138, pp. 417–429, 2014.

[38] E. Ghanbari, A. Saatchi, X. W. Lei, and D. D. Macdonald, "Studies on pitting corrosion of Al–Cu–Li alloys Part III: passivation kinetics of aa2098–t851 based on the point defect model," *Materials*, vol. 12, p. 1912, 2019.

[39] M. Navaser and M. Atapour, "Effect of friction stir processing on pitting corrosion and intergranular attack of 7075 aluminum alloy," *Journal of Materials Science & Technology*, vol. 33, no. 2, pp. 155–165, 2017.

[40] X. Y. Liu, M. J. Li, F. Gao, S. X. Liang, X. L. Zhang, and H. X. Cui, "Effects of aging treatment on the intergranular corrosion behavior of Al-Cu -Mg-Ag alloy," *Journal of Alloys and Compounds*, vol. 639, pp. 263–267, 2015.

[41] E. A. Ashour and B. G. Ateya, "Electrochemical behaviour of a copper aluminium alloy in concentrated alkaline solutions," *Electrochimica Acta*, vol. 42, no. 2, pp. 243–250, 1997.

[42] G. Williams, A. J. Coleman, and H. N. McMurray, "Inhibition of aluminium alloy AA2024-T3 pitting corrosion by copper complexing compounds," *Electrochimica Acta*, vol. 55, no. 20, pp. 5947–5958, 2010.

[43] J. G. Brunner, N. Birbilis, K. D. Ralston, and S. Virtanen, "Impact of ultrafine-grained microstructure on the corrosion of aluminium alloy AA2024," *Corrosion Science*, vol. 57, pp. 209–214, 2012.

[44] K. A. Yasakau, M. L. Zheludkevich, S. V. Lamaka, and M. G. S. Ferreira, "Mechanism of corrosion inhibition of AA2024 by rare-earth compounds," *Journal of Physical Chemistry B*, vol. 110, no. 11, pp. 5515–5528, 2006.

[45] U. Trdan and J. Grum, "SEM/EDS characterization of laser shock peening effect on localized corrosion of Al alloy in a near natural chloride environment," *Corrosion Science*, vol. 82, pp. 328–338, 2014.

[46] Y. Wang, Z. Q. Huang, Q. Yan et al., "Corrosion behaviors and effects of corrosion products of plasmaelectrolytic oxidation coated AZ31 magnesium alloy under the salt spray corrosion test," *Applied Surface Science*, vol. 378, pp. 435–442, 2016.

[47] Z. Ahmad, A. Ul-Hamid, and A. A. Bj, "The corrosion behavior of scandium alloyed Al 5052 in neutral sodium chloride solution," *Corrosion Science*, vol. 43, no. 7, pp. 1227–1243, 2001.

[48] J. Bockris and L. V. Minevski, "On the mechanism of the passivity of aluminum and aluminum alloys," *Journal of Electroanalytical Chemistry*, vol. 349, no. 1-2, pp. 375–414, 1993.

[49] L. Tomacsanyi, K. Varga, I. Bartik, G. Horanyi, and E. Maleczki, "Electrochemical study of the pitting corrosion of aluminium and its alloys-II.study of the interaction of chloride ions with, a passive film on aluminum and initiation of pitting corrosion," *Electrochimica Acta*, vol. 34, pp. 855–859, 1989.

[50] S. D. Wang, D. Xu, B. J. Wang et al., "Influence of phase dissolution and hydrogen absorption on the stress corrosion cracking behavior of Mg-7%Gd-5%Y-1%Nd-0.5%Zr alloy in 3.5 wt.% NaCl solution," *Corrosion Science*, vol. 142, pp. 185–200, 2018.